jove

Determining the Mechanical Strength of Ultra-Fine-Grained Metals

Jianing Xu[*,1,2], **Yanju Wang**[*,2], **Jinyuan Yan**[3], **Bin Chen**[1,2]

[1] School of Science, Harbin Institute of Technology [2] Center for High Pressure Science and Technology Advanced Research [3] Advanced Light Source, Lawrence Berkeley National Lab

[*] These authors contributed equally

Corresponding Author

Bin Chen
chenbin@hpstar.ac.cn

Citation

Xu, J., Wang, Y., Yan, J., Chen, B. Determining the Mechanical Strength of Ultra-Fine-Grained Metals. *J. Vis. Exp.* (177), e61819, doi:10.3791/61819 (2021).

Date Published

November 22, 2021

DOI

10.3791/61819

URL

jove.com/video/61819

Abstract

The mechanical strengthening of metals is the long-standing challenge and popular topic of materials science in industries and academia. The size dependence of the strength of the nanometals has been attracting a lot of interest. However, characterizing the strength of materials at the lower nanometer scale has been a big challenge because the traditional techniques become no longer effective and reliable, such as nano-indentation, micropillar compression, tensile, etc. The current protocol employs radial diamond-anvil cell (rDAC) X-ray diffraction (XRD) techniques to track differential stress changes and determine the strength of ultrafine metals. It is found that ultrafine nickel particles have more significant yield strength than coarser particles, and the size strengthening of nickel continues down to 3 nm. This vital finding immensely depends on effective and reliable characterizing techniques. The rDAC XRD method is expected to play a significant role in studying and exploring nanomaterial mechanics.

Introduction

The resistance to plastic deformation determines the materials' strength. The strength of the metals usually increases with the decreasing grain sizes. This size strengthening phenomenon can be well illustrated by the traditional Hall-Petch relationship theory from the millimeter down to submicron regime[1,2], which is based on the dislocation-mediated deformation mechanism of bulk-sized metals, i.e., dislocations pile up at grain boundaries (GBs) and hinder their motions, leading to the mechanical strengthening in metals[3,4].

In contrast, mechanical softening, often referred to as the inverse Hall-Petch relationship, has been reported for fine nanometals in the last two decades[5,6,7,8,9,10]. Therefore, the strength of the nanometals is still puzzling as continuous hardening was detected for grain sizes down to ~10 nm[11,12], while the cases of size softening below 10 nm regime were also reported[7,8,9,10]. The main difficulty or challenge

for this debated topic is to make statistically reproducible measurements on the mechanical properties of ultrafine nanometals and establish a reliable correlation between the strength and grain size of the nanometals. Another part of the difficulty comes from the ambiguity in the plastic deformation mechanisms of the nanometals. Various defects or processes at nanoscale have been reported, including dislocations[13,14], deformation twinning[15,16,17], stacking faults[15,18], GB migration[19], GB sliding[5,6,20,21], grain rotation[22,23,24], atomic bond parameters[25,26,27,28], etc. However, which one dominates the plastic deformation and thus determines the strength of nanometals is still unclear.

For these above issues, traditional approaches of mechanical strength examining, such as tensile test[29], Vickers hardness test[30,31], nano-indentation test[32], micropillar compression[33,34,35], etc. are less effective because the high quality of large pieces of nanostructured materials is so difficult to fabricate and conventional indenter is much larger than single nanoparticle of materials (for the single-particle mechanics). In this study, we introduce radial DAC XRD techniques[36,37,38] to material science to *in situ* track the yield stress and deformation texturing of nano nickel of various grain sizes, which are used in the geoscience field in previous studies. It has been found that the mechanical strengthening can be extended down to 3 nm, much smaller than the previously reported most substantial sizes of nanometals, which enlarges the regime of conventional Hall-Petch relationship, implying the significance of rDAC XRD techniques to material science.

Protocol

1. Sample preparation

1. Obtain 3 nm, 20 nm, 40 nm, 70 nm, 100 nm, 200 nm, and 500 nm nickel powder from commercial sources (see **Table of Materials**). The morphology characterization is shown in **Figure 1**.
2. Prepare 8 nm nickel particles by heating 3 nm nickel particles using a reaction kettle (see **Table of Materials**).
    1. Put ~20 mL of absolute ethanol and ~50 mg of 3 nm nickel powder into the reaction kettle.NOTE: The whole solution should not reach ~70% of the kettle volume.
    2. Heat the reaction kettle at 80 °C for 24 h.
    3. Cool the solution to room temperature and drop a little solution to one copper mesh (TEM grid, see **Table of Materials**).
    4. Put the dried copper mesh into the Transmission Electron Microscopy (TEM) chamber and observe the sample morphology under 200 kV voltage electron beam.
    NOTE: The copper mesh was air-dried for ~5 min or used a drying light of 5 min.
    5. Measure the particle size distribution from the TEM images manually.
    NOTE: The particle size measurement can also be done using any freely available software such as Image J.
    6. Take out the solution and vaporize the ethanol at room temperature; then, the rest of the black solid is

the pure nickel powder with an average particle size of 8 nm.

3. Prepare 12 nm nickel powder

    1. Repeat step 1.2, but change the "absolute ethanol" and "80 °C for 24 h" to "absolute isopropanol" and "150 °C for 12 h" to obtain the pure nickel powder with the average particle of 12 nm.

2. High-pressure radial DAC XRD measurements

1. Make X-ray transparent boron-epoxy gasket utilizing a laser drilling machine (see **Table of Materials**).

    1. Prepare Kapton (a kind of plastic) supporting gaskets

        NOTE: Kapton is a polyimide film material (see **Table of Materials**).

        1. Cut the inner circle with a laser drilling machine using the mentioned parameters: 35% laser power, three passes, 0.4 mm/s (cutting speed).
        2. Cut the outer rectangular using the parameters: 80% of laser power, two passes, 1.2 mm/s (cutting speed). The rectangular dimension is 8 x 1.4 mm.

    2. Prepare boron-epoxy gaskets from a larger boron disc with a diameter of ~10 mm.

        NOTE: The boron disc is made by compressing the mixture of amorphous boron powder and epoxy glue[36].

        1. Polish the raw discs to a thickness of 60-100 μm with sandpaper manually.

            NOTE: The sandpaper is from ~400 mesh to ~1000 mesh.

        2. Cut the inner circles with a laser drilling machine using the mentioned parameters: 35% laser power, three passes, 0.4 mm/s (cutting speed).
        3. Cut the outer circle with a laser drilling machine: 30% of laser power, one pass, 0.4 mm/s (cutting speed). Repeat and stop immediately when it comes off.

    3. Assemble the gaskets

        1. Place a Kapton supporting gasket (prepared in step 2.1.1) on a glass slide.
        2. Place a drilled boron gasket on the inner hole of the Kapton gasket. Ensure that the larger end of the boron gasket is at the top.
        3. Put another clean glass slide on the top. Hold it firmly and press it till the gasket is firmly inserted in the hole of Kapton gasket.
        4. Store the fabricated gasket assemblies between two clean glass slides and wrap them with glue tape for future use.

            NOTE: The gasket diameter, Ø = diamond culet size + 150 μm. For better reproducibility, the same setups can be used (possibly with small adjustments if something is found wrong) for the laser drilling and cutting during the gasket preparation. For good size matching, the diameter of gaskets entered for laser cutting is Ø + 23 μm while the diameter of the inner hole of the Kapton supporting gaskets (entered for laser cutting) is Ø - 23 μm.

2. Radial DAC experiment loading

    1. Mount the gasket assembly

1. On the viewing computer monitor (connected to the optical microscope), mark a dot to locate the center of the diamond (the piston diamond of the DAC).
2. Mount the boron-epoxy gasket (prepared in step 2.1) and the mark at the center of the gasket hole.
3. Use a glass slide to press down the gasket assembly such that the gasket firmly sets on the diamond of the piston.
   NOTE: A DAC has two identical pieces of diamonds. Generally, the upper one is called cylinder diamond, and the lower one is called piston diamond.

2. Cleaning and compacting the gasket setup
   1. Load samples with a chunk size smaller than the gasket hole such that there is no overflow of materials on the gasket surface.
      NOTE: The samples here mean the candidate materials that we studied in our experiments. In this study, the samples are different-sized Ni powders and Pt chips.
   2. Close the cell after the loading of a new piece of sample to achieve compactness.
3. Loading of soft materials (such as gold)
   1. Load only one piece of the soft sample (make the soft material as a small fraction of the loaded materials).
   2. Use hard amorphous materials to fill up the gasket hole for good compactness.
4. Loading of low atomic number materials (such as spinel, pyrope, serpentine)
   1. Mix the sample with 10% Pt or Au. Fill up the gasket hole with the mixture but without overflow.
   2. If necessary, put hard amorphous materials on the top for good compactness.
3. X-ray diffraction study
   1. Mount the X-ray transparent boron-Kapton gasket (prepared in step 2.1) with a thickness of 100 µm and a chamber hole of 60 µm on the top of 300 µm culet of DAC with the support of the clays.
   2. Place a small piece of Pt chip on top of the Ni sample as a pressure calibrant.
      NOTE: No pressure medium was used to maximize the differential stress between the axial and radial.
   3. Use a monochromatic synchrotron X-ray (see **Table of Materials**) with an energy of 25 or 30 keV to conduct the x-ray diffraction experiments.
   4. Focus the X-ray beam to ~30 x 30 μm^2 surface area on the sample.
   5. Collect the X-ray diffraction patterns at pressure intervals of 1-2 GPa by a two-dimension image plate (see **Table of Materials**) with a resolution of 100 µm/pixel. The setup used is shown in **Figure 2** and **Figure 3**.
4. The experimental data analysis
   1. Process each X-ray diffraction image into a file containing 72 spectra over 5° azimuthal steps using Fit2d[37,38,39,40,41,42].
      NOTE: A two-dimensional diffraction image contains 360° information. To analyze the stress and texture information, it is needed to separate into 72 files with 5° azimuthal information contained in each one.

Fit2d is the software used to analyze X-ray diffraction data[37,38,39,40,41,42].

2. Refine the diffraction pattern with the Rietveld method in the MAUD[37] software. The lattice strain of each lattice plane was obtained by fitting the pattern[37,40].

3. Calculate the differential stress and yield strength according to the lattice strain theory[38] and von Mises yield criterion[38,39] following step 2.5.

5. The lattice strain theory for the experimental data analysis

1. Determine the differential stress (the difference between these maximum ($\sigma_{22} = \sigma_{33}$) and minimum stress ($\sigma_{11}$) components) that provides a lower-bound estimate of a material's yield strength[38], σ_y, based on the von Mises yield criterion following equation (1)[38]:

(1) $t = \sigma_{11} - \sigma_{33} < 2\tau = \sigma_y$.

2. Obtain the direction-dependent deviatoric strain Q_{hkl} by measuring the d-spacings from different diffraction directions by following equation (2)[38]:

(2) $Q_{hkl} = (d_{0^\circ} - d_{90^\circ})/(d_{0^\circ} + 2d_{90^\circ})$

where d_{0° and d_{90° are the d-spacings measured from Ψ = 0° and Ψ = 90° (the angle between the diffraction vector and load axis), respectively.

3. Then, derive the value of t using equation (3)[38]:

(3) $$t = \frac{3Q_{hkl}}{\alpha\left[(2G_R(hkl))^{-1}\right] + (1-\alpha)(2G_V)^{-1}}$$

where $G_R(hkl)$ and G_V are the shear modulus of the aggregates under the Reuss (iso-stress) condition and Voigt (iso-strain) condition, respectively; α is the factor to determine the relative weight of Reuss and Voigt conditions[40].

NOTE: Considering the current experiments' complicated stress/strain conditions, α = 0.5 is used in this study.

4. For a cubic system, calculate $G_R(hkl)$ and G_V as follows using equations 4-6[38,40,41]:

(4)

$$[2G_R^X(hkl)]^{-1} = \left[S_{11} - S_{12} - 3(S_{11} - S_{12} - \frac{1}{2}S_{44})\Gamma(hkl)\right]$$

(5) $\Gamma(hkl) = (h^2k^2 + k^2l^2 + l^2h^2)/(h^2 + k^2 + l^2)^2$

(6) $(2G_V)^{-1} = \frac{5}{2}\frac{(S_{11}-S_{12})S_{44}}{[3(S_{11}-S_{12})+S_{44}]}$

where S_{ij} are the single crystal elastic compliances and can be obtained from the elastic stiffness constants C_{ij} of materials.

3. TEM measurements

1. Prepare thin pressurized Ni foils for TEM using a focused ion beam (FIB) system (see **Table of Materials**). To reduce possible artifacts during ion milling of the specimen, deposit a protective Pt layer using the Pt gun equipped in the SEM with a thickness of ~1 μm on the candidate region.

2. Perform TEM measurements on a 300 kV aberration-corrected transmission electron microscope equipped with high angle annular dark-field (HAADF) and bright-field (BF) detectors.

3. Take high-resolution TEM images.

Representative Results

Under hydrostatic compression, unrolled X-ray diffraction lines should be straight, not curved. However, under non-

hydrostatic pressure, the curvature (ellipticity of the XRD rings, which translates into the non-linearity of the lines plotted along the azimuth angle) significantly increases ultrafine-grained-nickel at similar pressures (**Figure 4**). At a similar pressure, the differential strain of the 3 nm sized nickel is the highest. The mechanical strength results (stress-strain curves) are shown in **Figure 5**. The strength continuously increases from coarser grains to finer grains, which is different from traditional knowledge[5,6,10] (inverse Hall-Petch relationship). After complete yield, the nano metals also have strong strain hardening.

The *in situ* captured deformation texture of nano nickel with various grain sizes at different pressures can also be obtained from the radial DAC XRD data[36]. In our previous study[36], larger nano grain sizes above 20 nm show very strong deformation texture even at low pressure. With grain size decreased below 20 nm, they show very weak deformation texture. It indicates that traditional total dislocation activity becomes less active in nano nickel below 20 nm. Naturally, other deformation mechanisms should take over the role of strengthening ultrafine nickel nanocrystals instead of the full dislocation slip.

To verify the partial slip deformation mechanism, TEM imaging measurements were conducted on the pressurized nickel crystals. As expected, high content of dislocations is seen in the coarse-grained sample (**Figure 6C**). In contrast, nano twins are well captured in the high pressure recovered nanocrystalline nickel, accompanied by some stacking faults[43] (**Figure 6A,B**). In short, twinning induced by stacking faults observed in the TEM measurements (**Figure 6**) originate from the nucleation and motion of partial dislocations[15]. This evidences that in the sub-10 nm particle size regime, the full-dislocation-mediated deformation shifts to the partial-dislocation-mediated deformation (with some degree of contribution of complete dislocation) in high-pressure compression.

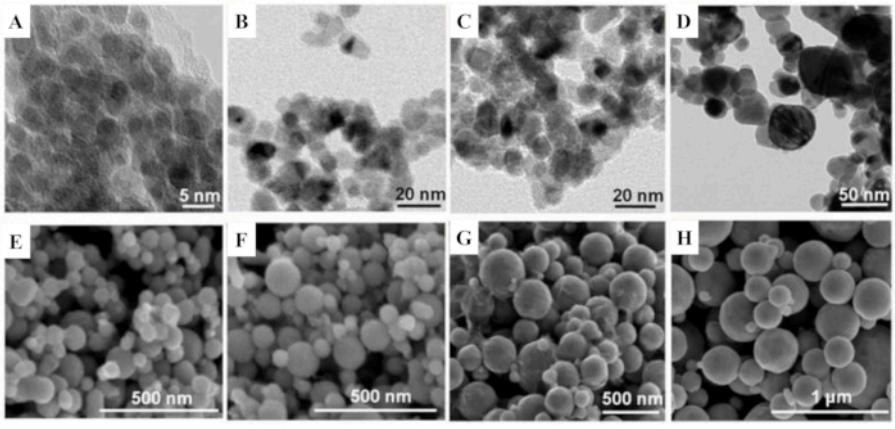

Figure 1: TEM and SEM images. TEM and SEM characterization of raw 3 nm (**A**), 8 nm (**B**), 12 nm (**C**), 20 nm (**D**), 40 nm (**E**), 70 nm (**F**), 100 nm (**G**), and 200 nm (**H**) nickel samples before compression. This figure has been adapted from Reference[36]. Please click here to view a larger version of this figure.

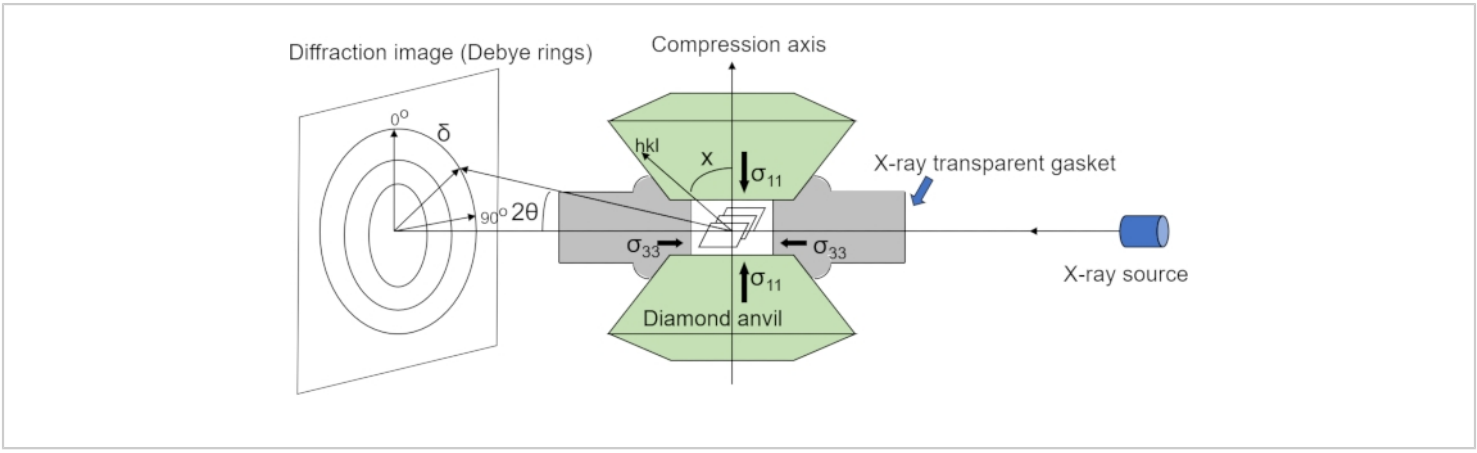

Figure 2: The experimental setup of radial DAC XRD. This figure has been adapted from Reference[36]. Please click here to view a larger version of this figure.

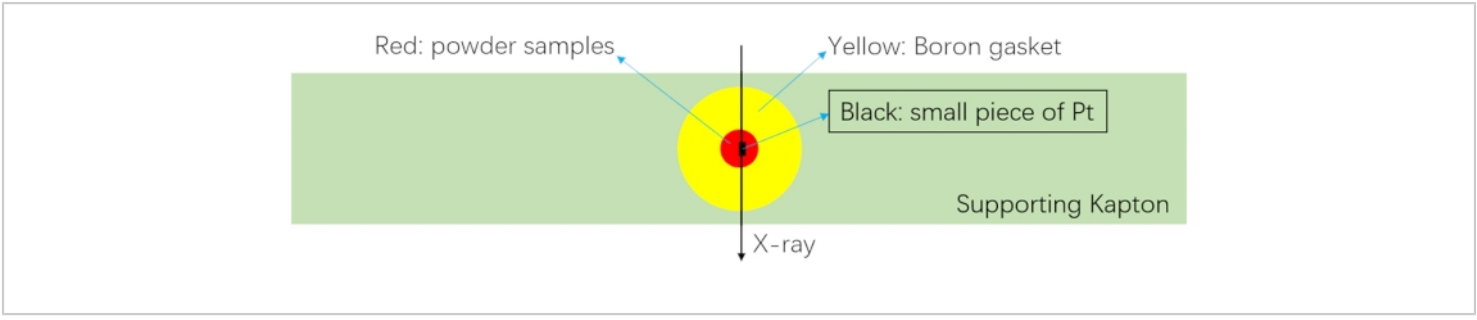

Figure 3: The top view of the sample chamber. The culet of the diamond needs to be smaller than the boron gasket (yellow part). Please click here to view a larger version of this figure.

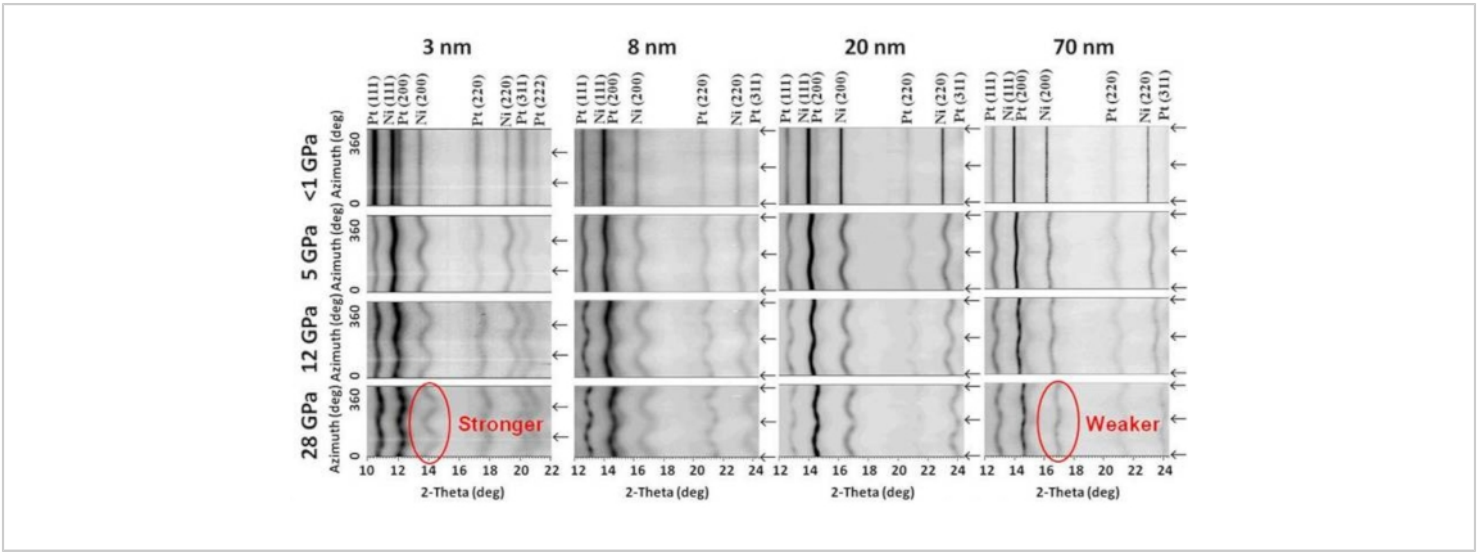

Figure 4: Azimuthally (0~360°) unrolled diffraction images of nickel at different pressures. The black arrows indicate the axial compression direction. At similar pressures, the curvature of diffraction lines increases with the decreasing grain size, suggesting the continuously mechanical strengthening. This figure has been adapted from Reference[36]. Please click here to view a larger version of this figure.

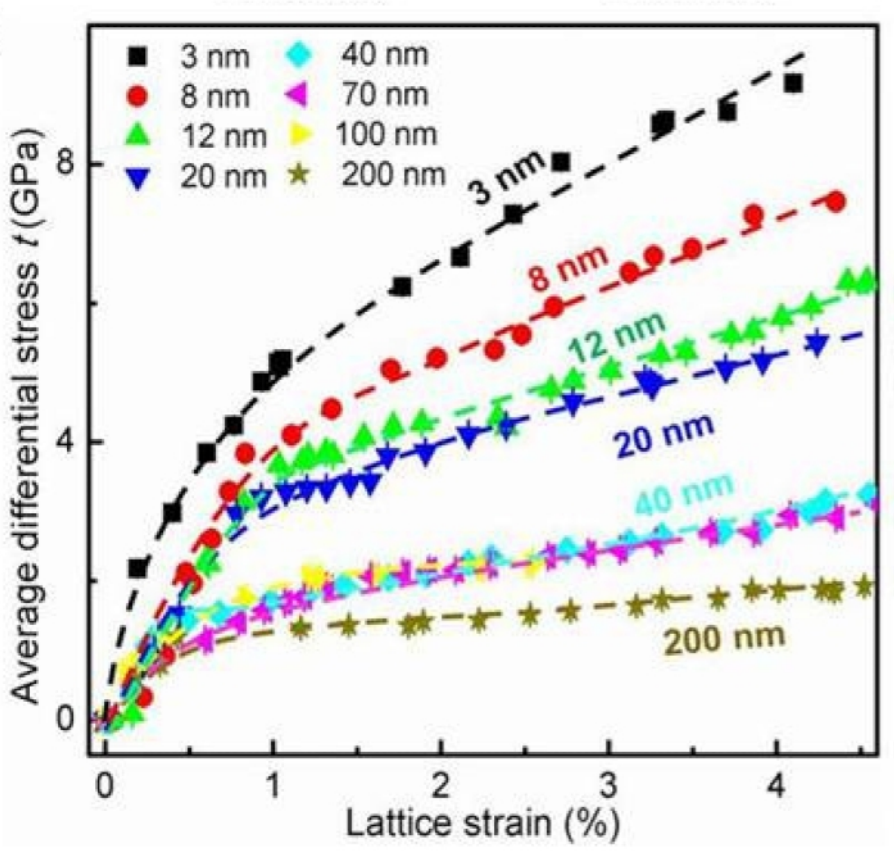

Figure 5: Size strengthening of nickel. From 200 nm to 3 nm, the nickel strengths (differential stress) always increase, reflecting the Hall-Petch relationship. This figure has been adapted from Reference[36]. Please click here to view a larger version of this figure.

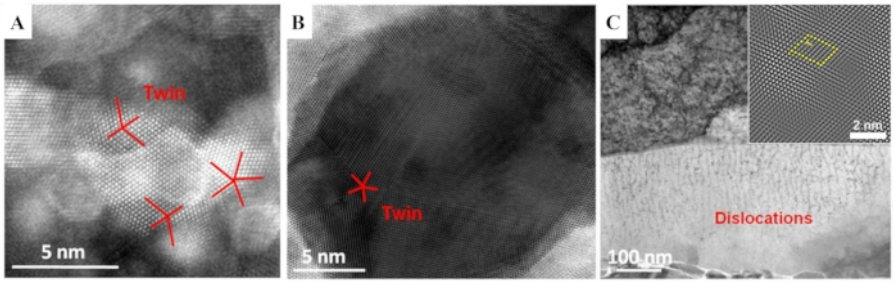

Figure 6: TEM observations of representative nickel quenched from around 40 GPa. (**A**) 3 nm Ni. (**B**) 20 nm Ni. (**C**) 200 nm Ni. Partial dislocation-induced twins can be seen in nickel below 20 nm, while lots of perfect dislocation lines are observed in coarser grains. An edge dislocation (yellow "T") is labeled in the inset of (**C**). Please click here to view a larger version of this figure.

Discussion

Computational simulations have been widely employed to study the grain size effect on the strength of nanometals[5,6,16,17,27,42]. Perfect dislocations, partial dislocations, and GB deformation have been proposed to play decisive roles in the deformation mechanisms of the nanomaterials. In a molecular dynamics simulation, Yamakov et al.[42] proposed a deformation mechanism map, including perfect dislocation, partial dislocation, and GB deformation, which depends on SF energy, the material's elastic properties, and the magnitude of the applied stress. Swygenhoven et al.[27] thought that slip in nano metals cannot be described in terms of the absolute value of SF energy but should be the generalized planar fault (GPF) energy involving stable and unstable SF energies. Jo et al.[44] found that different deformation modes, i.e., full slip, twinning, and SFs, are activated in different fcc metals by varying shear directions based on the GPF theory. These studies proposed that size softening would occur due to the dislocation-mediated to GB-mediated mechanism transition. However, these simulations cannot explain our observed size strengthening of sub-10 nm nickel nanocrystals. The current measurements indicate that the size strengthening is stronger in the smaller size range of nano nickel. Because perfect dislocations exist both in coarse- and fine-grained nickel, perfect dislocation cannot be the main strengthening reason. The slip of partial dislocations and the suppression of grain boundaries play an essential role in this extreme strengthening. The strength of the nano Pd and nano Au using were also measured using the same approach. These results confirm that the size strengthening phenomenon in ultrafine-grained metals is universal with high-pressure suppression of grain boundary activities.

These results also emphasize the importance of radial DAC XRD experimentation[14,38,43] in characterizing the mechanical performance of the nanomaterials. The high quality of large pieces (mm dimension and above) of real nanometer-grain-sized (below the critical grain size of 10 nm) metals is exceedingly difficult to manufacture because of grain coarsening and purity, even though severe plastic deformation (SPD) or equal channel angular pressing (ECAP) method. Therefore, there are few experimental

mechanical measurements on sub-10 nm grained metals to reveal the strengthening phenomenon[30]. Most inverse Hall-Petch relationship studies are reported by simulations[6]. The miniature tensile test requires a sample size of millimeter-level or above[45,46]. This bulk geometry size of a millimeter (even sub mm, with the grain size below 10 nm sized polycrystalline metals, is hard to obtain their repeatable mechanical properties. Moreover, the mechanics of highly pure metal nano-powders cannot be measured directly by conventional approaches (tension or compression test). With synchrotron-based X-ray and radial DAC, the repeatable and reliable mechanical results of real nano-grain-sized (sub 10 nm) metal powders can be obtained. We firstly introduced rDAC XRD technique from geoscience to material science. This should be a significant breakthrough in the mechanical characterization of nanometals.

Compressive strength measurements with radial DAC XRD allow statistically examining the mechanical properties of even sub-10 nm grain-sized metals[47,48]. The results are reproducible and reliable because of the excellent data statistics. This method[47,48] would have more extended applications not only in geoscience but also in material science. Except for the advantages of the high-pressure radial DAC XRD techniques, they also have their limitations on strength measuring. They are usually used for powder or polycrystalline samples because of the established lattice strain theory[38]. The high-pressure diffraction data of a single crystal is challenging to analyze. On the other hand, a non-hydrostatic high-pressure environment is needed to deform the samples, and the chamber is also small (<100 μm).

In summary, it was observed that other than the size softening in metals, known as the inverse Hall-Petch effect, the size strengthening can be extended down to 3 nm, much lower than that predicted by the established knowledge. Radial DAC XRD techniques are emphasized for evaluating the mechanical strength of the nanomaterials. The TEM observations reveal that the strengthening mechanisms shift from total dislocation-mediated plastic deformation to partial dislocation-associated plastic deformation. This finding encourages the efforts to achieve an even higher strength of materials by engineering grain sizes and grain boundary deformation suppression. This is expected to advance the industrial applications of nanometals further.

Disclosures

The authors have nothing to disclose.

Acknowledgments

We acknowledge support from the National Natural Science Foundation of China (NSFC) under grant numbers 11621062, 11772294, U1530402, and 11811530001. This research was also partially supported by the China Postdoctoral Science Foundation (2021M690044). This research used the resources of the Advanced Light Source, which is a DOE Office of Science User Facility under contract number DE-AC02-05CH11231 and the Shanghai Synchrotron Radiation Facility. This research was partially supported by COMPRES, the Consortium for Materials Properties Research in Earth Sciences under NSF Cooperative Agreement EAR 1606856.

References

1. Hall, E. O. The Deformation and ageing of mild steel.3. Discussion of results. *Proceedings of the Physical Society of London Section B.* **64** (381), 747-753 (1951).
2. Conrad, H. Effect of grain size on the lower yield and flow stress of iron and steel. *Acta Metallurgica.* **11** (1), 75-77 (1963).

3. Kanninen, M. F., Rosenfield, A. R. Dynamics of dislocation pile-up formation. *The Philosophical Magazine: A Journal of Theoretical Experimental and Applied Physics.* **20** (165), 569-587 (1969).
4. Thompson, A. A. W. Yielding in nickel as a function of grain or cell size. *Acta Metallurgica.* **23** (11), 1337-1342 (1975).
5. Schiotz, J., Di Tolla, F. D., & Jacobsen, K. W. Softening of nanocrystalline metals at very small grain sizes. *Nature.* **391** (6667), 561-563 (1998).
6. Schiotz, J., Jacobsen, K. W. A maximum in the strength of nanocrystalline copper. *Science.* **301** (5638), 1357-1359 (2003).
7. Conrad, H.,Narayan, J. Mechanism for grain size softening in nanocrystalline Zn. *Applied Physics Letters.* **81** (12), 2241-2243 (2002).
8. Chokshi, A. H., Rosen, A., Karch, J., Gleiter, H. On the validity of the hall-petch relationship in nanocrystalline materials. *Scripta Metallurgica.* **23** (10), 1679-1683 (1989).
9. Sanders, P. G., Eastman, J. A., Weertman, J. R. Elastic and tensile behavior of nanocrystalline copper and palladium. *Acta Materialia.* **45** (10), 4019-4025 (1997).
10. Conrad, H., Narayan, J. On the grain size softening in nanocrystalline materials. *Scripta Materialia.* **42** (11), 1025-1030 (2000).
11. Chen, J., Lu, L., Lu, K. Hardness and strain rate sensitivity of nanocrystalline Cu. *Scripta Materialia.* **54** (11), 1913-1918 (2006).
12. Knapp, J. A., Follstaedt, D. M. Hall-Petch relationship in pulsed-laser deposited nickel films. *Journal of Materials Research.* **19** (1), 218-227 (2004).
13. Kumar, K. S., Suresh, S., Chisholm, M. F., Horton, J. A., Wang, P. Deformation of electrodeposited nanocrystalline nickel. *Acta Materialia.* **51** (2), 387-405 (2003).
14. Chen, B. et al. Texture of Nanocrystalline Nickel: Probing the lower size limit of dislocation activity. *Science.* **338** (6113), 1448-1451 (2012).
15. Chen, M. W. et al. Deformation twinning in nanocrystalline aluminum. *Science.* **300** (5623), 1275-1277 (2003).
16. Yamakov, V., Wolf, D., Phillpot, S. R.,Gleiter, H. Deformation twinning in nanocrystalline Al by molecular-dynamics simulation. *Acta Materialia.* **50** (20), 5005-5020 (2002).
17. Yamakov, V., Wolf, D., Phillpot, S. R., Mukherjee, A. K., Gleiter, H. Dislocation processes in the deformation of nanocrystalline aluminium by molecular-dynamics simulation. *Nature Materials.* **1** (1), 45-49 (2002).
18. Yamakov, V., Wolf, D., Salazar, M., Phillpot, S. R., Gleiter, H. Length-scale effects in the nucleation of extended dislocations in nanocrystalline Al by molecular-dynamics simulation. *Acta Materialia.* **49** (14), 2713-2722 (2001).
19. Shan, Z. W. et al. Grain boundary-mediated plasticity in nanocrystalline nickel. *Science.* **305** (5684), 654-657 (2004).
20. Li, H. et al. Strain-Dependent Deformation Behavior in Nanocrystalline Metals. *Physical Review Letters.* **101** (1), 015502 (2008).
21. Van Swygenhoven, H., Derlet, P. M. Grain-boundary sliding in nanocrystalline fcc metals. *Physical Review B.* **64** (22), 224105(2001).

22. Ovid, ko, I. A. Deformation of nanostructures. *Science.* **295** (5564), 2386 (2002).
23. Murayama, M., Howe, J. M., Hidaka, H., Takaki, S. Atomic-level observation of disclination dipoles in mechanically milled, nanocrystalline Fe. *Science.* **295** (5564), 2433 (2002).
24. Wang, L. et al. Grain rotation mediated by grain boundary dislocations in nanocrystalline platinum. *Nature Communications.* **5,** 4402 (2014).
25. Edalati, K. et al. Influence of dislocation-solute atom interactions and stacking fault energy on grain size of single-phase alloys after severe plastic deformation using high-pressure torsion. *Acta Materialia.* **69**, 68-77 (2014).
26. Edalati, K., Horita, Z. High-pressure torsion of pure metals: Influence of atomic bond parameters and stacking fault energy on grain size and correlation with hardness. *Acta Materialia.* **59** (17), 6831-6836 (2011).
27. Yamakov, V., Wolf, D., Phillpot, S. R., Mukherjee, A. K., Gleiter, H. Deformation-mechanism map for nanocrystalline metals by molecular-dynamics simulation. *Nature Materials.* **3** (1), 43-47 (2004).
28. Starink, M. J., Cheng, X., Yang, S. Hardening of pure metals by high-pressure torsion: A physically based model employing volume-averaged defect evolutions. *Acta Materialia.* **61** (1), 183-192 (2013).
29. Yang, T. et al. Ultrahigh-strength and ductile superlattice alloys with nanoscale disordered interfaces. *Science.* **369** (6502), 427 (2020).
30. Hu, J., Shi, Y. N., Sauvage, X., Sha, G.,Lu, K. Grain boundary stability governs hardening and softening in extremely fine nanograined metals. *Science.* **355** (6331), 1292 (2017).
31. Yue, Y. et al. Hierarchically structured diamond composite with exceptional toughness. *Nature.* **582** (7812), 370-374 (2020).
32. Li, X. Y., Jin, Z. H., Zhou, X.,Lu, K. Constrained minimal-interface structures in polycrystalline copper with extremely fine grains. *Science.* **370** (6518), 831 (2020).
33. Yan, S. et al. Crystal plasticity in fusion zone of a hybrid laser welded Al alloys joint: From nanoscale to macroscale. *Materials and Design.* **160**, 313-324 (2018).
34. Khalajhedayati, A., Pan, Z., Rupert, T. J. Manipulating the interfacial structure of nanomaterials to achieve a unique combination of strength and ductility. *Nature Communications.* **7** (1), 10802 (2016).
35. Chen, L. Y. et al. Processing and properties of magnesium containing a dense uniform dispersion of nanoparticles. *Nature.* **528** (7583), 539-543 (2015).
36. Zhou, X. et al. High-pressure strengthening in ultrafine-grained metals. *Nature.* **579** (7797), 67-72 (2020).
37. Lutterotti, L., Vasin, R., Wenk, H.-R. Rietveld texture analysis from synchrotron diffraction images. I. Calibration and basic analysis. *Powder Diffraction.* **29** (1), 76-84 (2014).
38. Singh, A. K., Balasingh, C., Mao, H. K., Hemley, R. J., Shu, J. F. Analysis of lattice strains measured under nonhydrostatic pressure. *Journal of Applied Physics.* **83** (12), 7567-7575, (1998).
39. Hemley, R. J. et al. X-ray imaging of stress and strain of diamond, iron, and tungsten at megabar pressures. *Science.* **276** (5316), 1242-1245 (1997).

40. Merkel, S. et al. Deformation of polycrystalline MgO at pressures of the lower mantle. *Journal of Geophysical Research-Solid Earth.* **107** (B11), 2271 (2002).

41. Singh, A. K. The lattice strains in a specimen (cubic system) compressed nonhydrostatically in an opposed Anvil device. *Journal of Applied Physics.* **73** (9), 4278-4286 (1993).

42. Van Swygenhoven, H., Derlet, P. M., Frøseth, A. G. Stacking fault energies and slip in nanocrystalline metals. *Nature Materials.* **3** (6), 399-403 (2004).

43. Chung, H. Y. et al. Synthesis of ultra-incompressible superhard rhenium diboride at ambient pressure. *Science.* **316** (5823), 436-439 (2007).

44. Jo, M. et al. Theory for plasticity of face-centered cubic metals. *Proceedings of the National Academy of Sciences.* **111** (18), 6560 (2014).

45. Klueh, R. L. Miniature tensile test specimens for fusion reactor irradiation studies. *Nuclear Engineering and Design. Fusion.* **2** (3), 407-416 (1985).

46. Konopík, P., Farahnak, P., Rund, M., Džugan, J., Rzepa, S. Applicability of miniature tensile test in the automotive sector. *IOP Conference Series: Materials Science and Engineering.* **461**, 012043 (2018).

47. Yang, J. et al. Strength enhancement of nanocrystalline tungsten under high pressure. *Matter and Radiation at Extremes.* **5** (5), 058401 (2020).

48. Chen, B. Exploring nanomechanics with high-pressure techniques. *Matter and Radiation at Extremes.* **5** (6) (2020).